REMARKS

Reconsideration and withdrawal of the rejections set forth in the Office Action dated October 17, 2007 are respectfully requested in view of the following remarks.

I. Claim Amendments

Support for the amendments to claim 1 is found, for example, on page 8, paragraph [0039], of the specification.

II. Rejection Under 35 U.S.C. § 112, Written Description

Claims 1, 3 and 4 were rejected under 35 U.S.C. §112 as allegedly failing to comply with the written description requirement.

The rejection is respectfully traversed in view of the claim amendments and the following remarks.

It is the Examiner's position that "Applicant has not provided any specific identifying structural characteristics so that one skilled in the art can correlate the interferon-tau analogs, fragments, and variants encompassed by the claims with a distinct biological function." (page 4 of the Office Action dated October 17, 2007). Furthermore, the Examiner takes the position that "[t]he specification does not provide any disclosure regarding the number of amino acid changes, the identities of the amino acids, and the location of these changes for the claimed interferon-tau homologue while still retaining a biological function." (page 5 of the Office Action dated October 17, 2007).

The law allows patent applicants to put forward evidence of structural characteristics and amino acid changes that are not disclosed in the specification if this evidence is known by one of skill in the art:

> For some biomolecules, examples of identifying characteristics include a sequence, structure, binding affinity, binding specificity, molecular weight, and length. Although structural formulas provide a convenient method of demonstrating possession of specific molecules, other identifying characteristics or combinations of characteristics may demonstrate the

requisite possession. As explained by the Federal Circuit, "(1) examples are not necessary to support the adequacy of a written description; (2) the written description standard may be met ... even where actual reduction to practice of an invention is absent; and (3) there is no per se rule that an adequate written description of an invention that involves a biological macromolecule must contain a recitation of known structure." *Falkner v. Inglis*, 448 F.3d 1357, 1366, 79 USPQ2d 1001, 1007 (Fed. Cir. 2006). See also *Capon v. Eshhar*, 418 F.3d at 1358, 76 USPQ2d at 1084 ("The Board erred in holding that the specifications do not meet the written description requirement because they do not reiterate the structure or formula or chemical name for the nucleotide sequences of the claimed chimeric genes" where the genes were novel combinations of known DNA segments.).(M.P.E.P. 2163, II, A, 3(a))

When the application was filed, the identifying structural characteristics that allow one of skill in the art to correlate the interferon-tau analogs, fragments, and variants encompassed by the claims with a distinct biological function were well-known in the art. Two publications, which are included as Exhibits 1 and 2, describe many of the structural features of interferon-tau that would enable one of skill in the art to make the peptides of the claimed subject matter.

Pontzer, C. *et al.* "Structure/Function Studies with Interferon Tau: Evidence for Multiple Active Sites" *J. Interferon Res.*, 14:133-141 (1994), provide data that correlate the structure of ovine interferon-tau with regions that exhibit antiviral activity. (Exhibit 1) Both interferon-tau and interferon-alpha interact with the type I interferon receptor. (Exhibit 1, page 136, left column) Peptide fragments of interferon-tau can compete with interferon-alpha interactions with the receptor. For instance, peptides corresponding to ovine interferon-tau amino acid residues 62-92, amino acid residues 119-150, and residues 139-172 all competed with interferon-alpha, suggesting that they were able to interact with the type I interferon receptor. The authors explain this result by stating that these peptides correspond to three antiviral regions of ovine interferon-tau. (Exhibit 1, page 139, left column) Two peptide fragments, corresponding to residues 34-64 and

90-122, did not compete with interferon-alpha (Exhibit 1, Fig. 1, and page 135). Antisera generated against the residues 34-64 and 90-122 were not able to reduce interferon-tau antiviral activity. (Exhibit 1, page 136, left column)

Based on this disclosure, one of skill in the art could design peptides with 90% sequence identity to SEQ ID NO: 2 that possess antiviral activity. Based on the disclosure in Exhibit 1, one skilled in the art would appreciate the areas of the peptide that may be modified without disturbing the activity of the peptide.

Radhakrishnan, R. *et al.* "Crystal Structure of Ovine Interferon-tau at 2.1 Angstrom Resolution" J. Mol. Biol., 286:151-162 (1999), disclose the crystal structure of interferon-tau. The structure of interferon-tau is comprised of five alpha helices and four loop domains that join these helices. (Exhibit 2, page 153, left column) With the disclosure that the structure of interferon-tau is comprised of alpha-helices, one of skill in the art could make selective mutations in SEQ ID NO: 2 that would tend to preserve the helical folding and antiviral activity such that homologues with 90% sequence identity to SEQ ID NO: 2 are fully enabled.

Radhakrishnan et al. disclose a variety of single amino acids that play a role in forming the overall ovine interferon-tau structure. These include, in order: Cys1, Leu7, Asn14, Asn22, Arg23, Leu24, Ser25, Asp35, Gly37, Leu38, Gln40, Phe54, Leu57, Ser64, Tyr69, Glu71, His72, Trp77, Cys86, Gln92, Leu96, Cys99, Tyr123, Gly135, Tyr136, Ser137, Cys139, Ala140, Glu142, Arg145, Glu147, Ser151, Ser155, Thr156, Gln159, and Leu162. (disclosed throughout Exhibit 2) One of skill in the art would know how to use the above information on single amino acids to create effective homologues with 90% sequence identity to SEQ ID NO: 2.

In conclusion, the disclosures of Pontzer et al. and Radhakrishnan et al. would allow one of skill in the art to know which peptides having at least 90% sequence identity to SEQ ID NO: 2 would retain biological activity. Accordingly, Applicants respectfully request withdrawal of the rejection under 35 U.S.C. §112, first paragraph.

Accordingly, Applicants respectfully request withdrawal of the rejection under 35 U.S.C. §112, first paragraph.

III. Rejection Under 35 U.S.C. § 112, Enablement

Claims 1, 3 and 4 were rejected under 35 U.S.C. §112 as allegedly failing to comply with the enablement requirement.

It is the Examiner's position that the specification is enabling for a method of treating a patient with multiple sclerosis by reducing the blood level of interferon-gamma by administering the interferon-tau protein comprising the amino acid sequence of SEQ ID NO: 2 or 3. It is also the Examiner's position that the specification does not teach any interferon homologues at least 80% identical to ovine interferon-tau that maintain their biological activities in order to decrease interferon-gamma blood levels.

The Radhakrishnan and Pontzer references discussed above provide structural characteristics for any interferon-tau of the claimed subject matter, i.e. having at least 90% sequence identity to SEQ ID NO: 2. (Exhibits 1 and 2) These references were part of the state of the art at the time of the filing of the instant application.

As discussed above, these references disclose structural features of ovine interferon-tau that are correlated with biological activity. These features include regions of ovine interferon-tau that interact with the type I interferon receptor, the crystal structure which discloses the five alpha helices and amino acid residues thought to play a role in forming the overall structure. Armed with this structural information, one of skill in the art can design molecules with 90% sequence identity to SEQ ID NO: 2 that will retain biological activity, without undertaking undue experimentation.

Accordingly, Applicants respectfully request withdrawal of the rejection under 35 U.S.C. §112, first paragraph.

IV. Rejection Under 35 U.S.C. § 112, New Matter

Claims 1, 3 and 4 were rejected under 35 U.S.C. §112 as allegedly claiming subject matter not described in the specification. The rejection is respectfully traversed in view of the claim amendments and the following remarks.

Claim 1 is now amended to be directed to an interferon-tau having greater than about 90% sequence identity to SEQ ID NO: 2. This claim amendment finds support on page 8, paragraph [0039] of the specification. Applicants respectfully submit that amended claim 1 does not claim subject matter not described in the specification.

V. Conclusion

In view of the foregoing, Applicants submit that the claims pending in the application are fully in condition for allowance. A Notice of Allowance is, therefore, respectfully requested. If the Examiner has any questions or believes a telephone conference would expedite prosecution of this application, the Examiner is encouraged to call the undersigned at (650) 838-4300.

Respectfully submitted,
Perkins Coie LLP

Date: 2/19/2008

Daniel A. Rube
Registration No. 53,536

Correspondence Address:
Customer No. 22918

JOURNAL OF INTERFERON RESEARCH 14:133–141 (1994)
Mary Ann Liebert, Inc., Publishers

Exhibit 1

Structure/Function Studies with Interferon Tau: Evidence for Multiple Active Sites

CAROL H. PONTZER,[1,2] TROY L. OTT,[4] FULLER W. BAZER,[4] and HOWARD M. JOHNSON[2,3]

ABSTRACT

A novel interferon (IFN), called IFN-tau (IFN-τ), has recently been discovered and has been shown to be a pregnancy recognition hormone. Unlike known IFNs, however, IFN-τ exhibits high antiviral and antiproliferative activity without cytotoxicity. The structural basis for IFN-τ function has been examined using six overlapping synthetic peptides corresponding to the entire ovine (Ov) IFN-τ sequence. Four peptides representing amino acids 1–37, 62–92, 119–150, and 139–172 inhibited OvIFN-τ antiviral activity in a dose-dependent manner. Polyclonal antipeptide antisera directed against the same four peptides blocked OvIFN-τ binding and antiviral activity, confirming the specificity of the peptide competitions. Because IFN-τ and IFN-α both interact with the type I IFN receptor, peptide inhibition of bovine and human IFNα activity was also determined. Of importance, only three peptides, OvIFN-τ(62–92), (119–150), and (139–172) inhibited IFN-α antiviral activity. The amino-terminal IFN-τ peptide, OvIFN-τ(1–37), was not inhibitory. These data suggest that the internal and carboxy-terminal reactive domains of IFN-τ may interact with a common type I IFN site on the receptor, while the amino terminus interacts with a site that elicits activity unique to OvIFN-τ. Finally, the antiproliferative activity of OvIFN-τ was localized primarily to the broad carboxy-terminal region, with OvIFN-τ(119–150) being the most effective inhibitor of OvIFN-τ-induced reduction of cell proliferation. Thus, multiple domains of IFN-τ have functional significance. Furthermore, because the amino-terminus of the molecule appears to interact with the type I IFN receptor in an IFN-τ-specific manner, modified IFN-τ or IFN-τ/IFN-α chimeras may be produced with selective biological activity.

INTRODUCTION

OVINE INTERFERON-TAU (OvIFN-τ) belongs to a newly described class of IFNs that display the remarkable property of signaling maternal recognition of pregnancy.[1] The IFN-τs are produced by an unusual source, the trophoblast of the conceptus, and in much greater quantities than observed for other IFNs. Initially, OvIFN-τ was found to exhibit 50–70% identity with IFNs-α of various species, but was 172 amino acids in length as compared with 166 for the IFNs-α.[2] Furthermore the IFNs-τ are not readily inducible by virus, and the transcriptional activator IRF-1, which binds all other type I IFN promoters, failed to affect an IFN-τ promoter.[3] The IFNs-τ have been shown to bind to the type I IFN receptor as do IFN-α, IFN-β, and IFN-ω,[4] and upon binding they exhibit potent antiviral activity (2×10^8 units/mg protein), making them as potent as the majority of IFNs-α.[5] Antiviral activity of OvIFN-τ against feline immunodeficiency virus (FIV) and human immunodeficiency virus (HIV), the causative agents of feline and human acquired immunodeficiency syndrome (AIDS), respectively, has also been demonstrated.[6] In addition to antiviral activity, OvIFN-τ displays anticellular activity.[7] Concentrations as low as 1 unit/ml inhibit the progress of cells through S phase. Most importantly, the antiviral and anticellular activity elicited by high doses of OvIFN-τ occurs in the absence of the cytotoxicity associated with high concentrations of IFN-α.[6,7] Although 10,000 units/ml of a consensus IFN-α (R & D Systems, Minneapolis, MN) or recombinant human IFN-α2A (Lee Biomolecular, San Diego, CA) routinely decrease the viability of normal human peripheral blood lymphocytes or eight different human tumor cell

[1]Department of Microbiology, University of Maryland, College Park, MD 20742; TEL: (301) 405-5435 FAX: (301) 314-9489; [2]PepTech, Inc., Alachua, FL 32615; [3]Department of Microbiology and Cell Science, University of Florida, Gainesville, FL 32611; [4]Department of Animal Science, Texas A & M University, College Station, TX 77843-2471.

lines, OvIFN-τ is not cytotoxic at this concentration (C.H.P., unpublished observation). Because IFN-α is currently used in treatment of viral diseases such as hepatitis, neoplasias such as hairy cell leukemia, and may have application to AIDS, IFN-τ may represent a significant therapeutic advance.

The pleiotropic nature of OvIFN-τ, its potency, and its lack of cytotoxicity all suggest the importance of structure/function analysis of this novel IFN. Using synthetic peptides corresponding to only the amino- and carboxy-terminal regions of the molecule, we have previously shown that the highly conserved carboxy-terminal region of the molecule is involved in binding to the type I IFN receptor.[6] In the present study, we extend our initial observations by examining the functional relevance of the entire IFN-τ sequence using overlapping synthetic peptides and their corresponding antipeptide antisera. Additional functional domains involved in antiviral and antiproliferative activity have been identified. These results suggest the possibility for the design of mutant IFN-τ molecules whose activity can be specifically targeted.

MATERIALS AND METHODS

Reagents: OvIFN-τ was obtained from *in vitro* cultures of day-16 (day 0 = first day of estrus) conceptuses and purified from the culture media by sequential anion-exchange and molecular sieve chromatography as described previously.[5] OvIFN-τ was homogeneous, as assessed by sodium dodecyl sulfate-polyacrylamide gel electrophoresis (SDS-PAGE). Recombinant IFN-τ was produced from a synthetic gene in *Saccharomyces cerevisiae*.[9] It is initially expressed as a fusion protein with ubiquitin and processed *in vivo* by an endogenous ubiquitin-cleaving enzyme. No differences were observed between the native and recombinant proteins in the assays performed. The bicinchoninic (BCA) assay (Pierce Chemical Co., Rockford, IL) was used for protein determinations. Recombinant bovine IFN-α_{II} (rBOvIFN-α) and recombinant bovine (rBoIFN-γ) were kindly supplied by Ciba-Geigy (Basel, Switzerland). The reference preparation of recombinant human IFN-α (rHuIFN-α) was supplied by the National Institutes of Health. All tissue culture media, sera, and IFNs used in this study were negative for endotoxin, as determined by assay with *Limulus* amebocyte lysate (Associates of Cape Cod, Woods Hole, MA) at a sensitivity level of 0.07 ng/ml.

Synthetic Peptides: Overlapping peptides corresponding to the entire OvIFN-τ sequence were synthesized on a Biosearch 9500AT automated peptide synthesizer using FMOC chemistry.[10] Peptides were cleaved from the resins using trifluoroacetic acid/ethanedithiol/thioanisole/anisole at a ratio of 90/3/5/2. After 1.5 h, Arg-pmc (2,2,5,7,8-pentamethylchroman-6-sulfonyl) deprotection is approximately 98% complete. In contrast, cysteine side chains were protected with acetamidomethyl, which would not be removed by this cleavage procedure, thus preventing the formation of inappropriate disulfide bonds. Cleaved peptides were then extracted in ether and ethyl acetate, dissolved in water, and lyophilized. The amino acid composition was verified by amino acid analysis and reverse-phase HPLC was employed for additional purification. Polyclonal antisera to each peptide were produced by hyperimmunization of rabbits. For immunization, peptides were conjugated to keyhole limpet hemocyanin using glutaraldehyde as the coupling reagent. Antisera titers to peptides or the native IFNτ molecule were assessed by enzyme-linked immunosorbent assay (ELISA), as previously described.[8]

Antiviral Assay: Activity is expressed as antiviral units/ml in a standard cytopathic effect assay.[11] Briefly, dilutions of the various IFNs were incubated with Madin–Darby bovine kidney (MDBK) cells for 16–18 h at 37°C. Following IFN treatment, inhibition of viral replication was determined by challenge with vesicular stomatitis virus (VSV). One antiviral unit caused a 50% reduction in destruction of the monolayer. The effect of peptides or antipeptide antisera was examined by addition of a range of IFN-τ peptide concentrations or antisera dilutions simultaneously with the IFNs.

OvTP-1 Binding: Five micrograms of OvIFN-τ was iodinated with 500 μCi of $Na^{125}I$ (15 mCi/μg; Amersham) using Iodo-Beads (Pierce). Radioiodinated OvIFN-τ was separated from free iodine on a 1 × 10-cm column of Sephadex G-10. The specific activity of the iodinated protein was 137 μCi/μg. For binding assays, monolayers of MDBK cells were fixed with 4% paraformaldehyde and blocked with 5% nonfat dry milk. Cells were incubated with 5 n*M* ^{125}I-OvIFN-τ in phosphate-buffered saline (PBS) with 1% bovine serum albumin (BSA) for 2 h at 4°C in the presence or absence of a 1:30 dilution of antipeptide antisera or the appropriate preimmune sera. Specific binding was assessed by incubation with a 100-fold molar excess of unlabeled OvIFN-τ. After incubation, the monolayers were washed three times, solubilized with 1% SDS, and the radioactivity counted.

Cell Cycle Analysis: MDBK cells were synchronized in G_0/G_1 phase by culturing confluent monolayers with minimum essential medium with Hank's salts (HMEM) containing 0.5% "spent" medium for an additional 7 days. For examination of OvIFN-τ activity, cells were replated at 2.5×10^5 cells/well in fresh HMEM containing 10% fetal bovine serum (FBS) in six-well plates. Various dilutions of IFNs alone or in combination with peptides were added to achieve a final volume of 1 ml. Plates were incubated at 37°C in 5% CO_2 for 24 or 48 h. For propidium iodide staining, cells were collected by trypsinization and washed. The cell pellet was blotted to dryness and 250 μl of nuclear staining solution (5 mg propidium iodide, 0.03 ml NP-40, and 0.1 gram sodium citrate in 100 ml of distilled H_2O) were added to each tube, followed by incubation at room temperature. After 10 min, 250 μl of RNase (500 units/ml in 1.12% sodium citrate) were added per tube, followed by an additional 20 min of incubation. Nuclei were filtered through 44-μm mesh and analyzed on a FACStar (Becton Dickinson, Mountain View, CA) using the DNA 2.0 software.

RESULTS

Overlapping synthetic peptides were synthesized corresponding to the entire OvIFN-τ sequence (Table 1). They were of approximately the same molecular weight but differed slightly in overall hydrophilicity. Despite this difference, all peptides, even the less hydrophilic carboxy-terminal peptide, were antigenic as demonstrated by the production of rabbit antisera with titers to the corresponding peptide greater than 1:10,000 when assessed by ELISA (data not shown). No cross-reactivity (titers < 1:10)

TABLE 1. OVERLAPPING OvIFN-τ PEPTIDES

Peptides	*M.W.*	*Hydropathic index*[a]	*Antisera and Titer*[b]	*Sequence*
OvIFN-τ(1–37)	4,465	−0.78	1:300	CYLSRKLMLDARENLKLLDRMNRLSPHSCLQDRKDFG
OvIFN-τ(34–64)	3,610	−0.72	1:1,000	KDFGLPQEMVEGDQLQKDQAFPVLYEMLQQS
OvIFN-τ(62–92)	3,586	−0.53	1:1,000	QQSFNLFYTEHSSAAWDTTLLEQLCTGLQQQ
OvIFN-τ(90–122)	3,712	−0.86	1:10,000	QQQLDHLDTCRGQVMGEEDSELGNMDPIVTVKK
OvIFN-τ(119–150)	3,948	−0.56	1:100	TVKKYFQGIYDYLQEKGYSDCAWEIVRVEMMR
OvIFN-τ(139–172)	3,818	−0.11	1:30	CAWEIVRVEMMRALTVSTTLQKRLTKMGGDLNSP

[a]Average hydropathicity values were calculated by taking the sum of the hydropathy values for each amino acid divided by the total number of amino acids in each sequence. Hydropathy values were taken from Kyte and Doolittle.[12]

[b]Titer of antipeptide antisera to native IFN-τ as assessed by ELISA. Titers reported represent the dilution of antipeptide antisera that produced twice the OD observed with the matching prebleed.

was observed between the antipeptide antisera and the noncorresponding IFN-τ peptides or an irrelevant peptide representing amino acids 1–27 of staphylococcal enterotoxin A. The antipeptide antisera were all reactive with the native IFN-τ molecule (Table 1). The antisera titers were roughly correlated with the hydropathic index of the peptide rather than with the predicted surface accessibility of the specific region in the three-dimensional configuration.[8]

The effect of IFN-τ peptides on the antiviral activity of OvIFN-τ was examined in a dose–response assay (Fig. 1). The most effective competitor of IFN-τ antiviral activity was the carboxy-terminal peptide OvIFN-τ(139–172). At 10^{-4} *M*, inhibition of antiviral activity was significantly different from control (no peptide) and all other IFN-τ peptides. Three additional peptides, OvIFN-τ (1–37), (62–92), and (119–150), also significantly reduced IFN-τ antiviral activity relative to control. This suggests that multiple regions of IFN-τ interact with the type I IFN receptor, and participate in the elicitation of antiviral activity. Two IFN-τ peptides corresponding to amino acids (34–64) and (90–122) were devoid of significant activity, even at 10^{-3} *M*. Addition of peptides in the absence of OvIFN-τ was without effect (data not shown). Thus, there are multiple domains of the OvIFN-τ molecule that are important for antiviral activity.

To verify functional results observed using the synthetic peptides, the ability of antipeptide antisera to inhibit OvIFN-τ an-

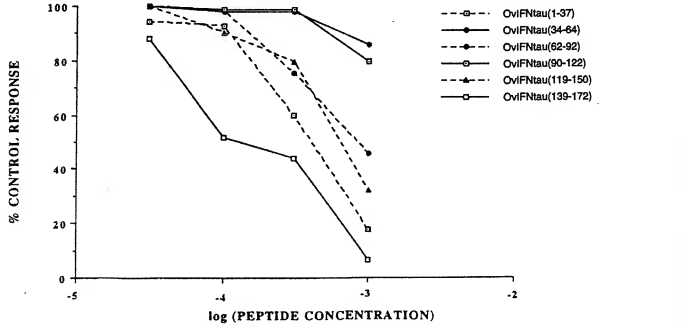

FIG. 1. Peptide inhibition of OvIFN-τ antiviral activity. Monolayers of MDBK cells were incubated with 40 units/ml of OvIFN-τ in the presence or absence of various concentrations of OvIFN-τ peptides. Results are expressed as the percent of control (without peptide) antiviral activity. Data presented are the means of six replicate experiments. OvIFN-τ(1–37), (62–92), (119–150), and (139–172) were significantly different than OvIFN-τ(34–64) and (90–122) at 10^{-3} *M* and 3×10^{-3} *M*. OvIFN-τ(139–172) was significantly different than all other peptides at 10^{-4} *M*. Significance was assessed by analysis of variance followed by Scheffe's *F*-test at $p < 0.05$.

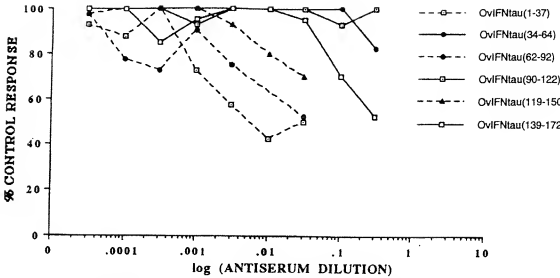

FIG. 2. Antipeptide antisera inhibition of OvIFN-τ antiviral activity. Monolayers of MDBK cells were incubated with 40 units/ml OvIFN-τ in the presence or absence of various dilutions of either preimmune or antipeptide antisera for 24 h. Representative results are expressed as the mean of triplicate determinations from a standard antiviral assay with vesicular stomatitis virus challenge. Data are presented as net percent of control (without antisera) antiviral activity, which is the percent inhibition produced by antipeptide antisera over that of the respective preimmune sera. Polyclonal antisera to OvIFN-τ(1–37), (62–92), (119–150), and (139–172) significantly inhibited OvIFN-τ antiviral activity relative to antisera against OvIFN-τ(34–64) and (90–122). Significance was assessed by analysis of variance followed by Scheffe's F-test at $p < 0.05$.

tiviral activity was also determined. Consistent with the peptide studies, antisera to OvIFN-τ(1–37), OvIFN-τ(62–92), OvIFN-τ (119–150), and OvIFN-τ(139–172) significantly inhibited IFN-τ antiviral activity in a dose-dependent manner, while antisera to OvIFN-τ(34–64) and OvIFN-τ(90–122) did not (Fig. 2). Levels of inhibition shown relative to control cultures without antisera represent reduction over and above that observed by addition of the matching prebleed. A prozone effect was observed with higher concentrations of the inhibitory antisera. The lack of effect of the two unreactive antisera was not a function of titer against OvIFN-τ, since both had equal or greater titer to the native OvIFN-τ molecule (Table 1). Conversely, anti-carboxy-terminal peptide antiserum was still an effective inhibitor despite its low titer, although the dilution producing half-maximal activity was shifted by approximately 1 log from the other three inhibitory antisera. These data are consistent with the previously reported ability of anti-carboxy-terminal peptide antisera to block binding of OvIFN-τ to its receptor on endometrial cells.[8] We have expanded this observation by examination of the effect of the full panel of anti-OvIFN-τ peptide antisera on OvIFN-τ binding to MDBK cells (Fig. 3). The same antisera that inhibited OvIFN-τ antiviral activity were also the most effective inhibitors of binding of ^{125}I-labeled OvIFN-τ to the type I IFN receptor. Thus, peptide competitions and antisera neutralizations both identify an amino-terminal, carboxy-terminal, and sequentially internal region of OvIFN-τ as all being involved in receptor binding and subsequent antiviral function.

Since IFN-τ and IFN-α both have been shown to bind to the type I IFN receptor, the ability of the IFN-τ synthetic peptides to block bovine and human IFN-α activity was examined (Figs. 4

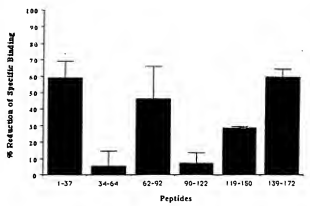

FIG. 3. Antipeptide antisera inhibition of ^{125}I-labeled OvIFN-τ binding. Monolayers of MDBK cells were incubated with 5 *nM* ^{125}I-labeled OvIFN-τ in the presence of a 1:30 dilution of either preimmune sera or antisera to OvIFN-τ peptides. Specific binding of 36% was determined by competition with 500 nM unlabeled OvIFN-τ. For example, total counts bound were 6,850 ± 133, and a 100-fold molar excess of OvIFN-τ produced 4,398 ± 158 counts per minute. Data from three replicate experiments are presented as the mean percent reduction of OvIFN-τ-specific binding produced by antipeptide antisera relative to the appropriate preimmune sera ± standard deviation. Antisera to OvIFN-τ(1–37), (62–92), and (139–172) were significantly different than antisera to OvIFN-τ(34–64) and (90–122) by Scheffe's F test at $p < 0.05$. Antisera to OvIFN-τ(119–150) was significantly different than antisera to OvIFN-τ(34–64) and (90–122) by Fisher's PLSD at $p < 0.05$.

and 5). The carboxy-terminal peptide of OvIFN-τ, OvIFN-τ (139–172), was the most effective competitor of IFN-α activity as was observed for IFN-τ. Additionally, OvIFN-τ(62–92) and (119–150) at 10^{-3} *M* also significantly inhibited bovine and human IFN-α antiviral activity relative to control and all other peptides. Of particular importance, the amino-terminal peptide OvIFN-τ(1–37) did not exhibit inhibitory activity against either bovine or human IFN-α. Thus, amino acids 62–92 and the broad carboxy-terminal region of IFN-τ may interact with the type I IFN receptor at a site shared with IFN-α. In contrast, the amino-terminal domain of IFN-τ and IFN-α appear to interact with receptor in different fashions. Either the IFN-α amino-terminus has a much higher affinity for receptor, or IFN-τ binds a unique region of the receptor complex that is most likely responsible for the unique properties of IFN-τ.

IFN-τ synthetic peptide inhibition of IFN-γ antiviral activity was examined as a control for the specificity of peptide effects. Bovine IFN-γ exhibits low sequence homology with OvIFN-τ. Furthermore, it interacts at an entirely different receptor, the type II IFN receptor. As seen in Fig. 6, none of the IFN-τ peptides blocked IFN-γ antiviral activity. In addition to the data obtained with antipeptide antisera, these IFN-γ data confirm the lack of nonspecific inhibitory effects, even at 10^{-3} *M* peptide.

In addition to antiviral activity, OvIFN-τ is also known to exhibit potent antiproliferative activity.[7] This inhibition of cell division occurs in the absence of toxicity, even at high concentrations. Functionally important sites for this antiproliferative activity of OvIFN-τ were also examined using synthetic peptides (Table 2). When proliferation of MDBK cells was monitored over a 2-day period, cell number increased roughly two-fold with greater than 95% viability. Cell proliferation was unaffected by the addition of OvIFN-τ-peptides alone (data not shown). In contrast, addition of 300 units/ml of OvIFN-τ entirely eliminated cell proliferation without a decrease in cell viability. The IFN-τ carboxy-terminal region peptides significantly reversed OvIFN-τ antiproliferative activity, with OvIFN-τ(119–150) > OvIFN-τ(90–122), and OvIFN-τ(139–172). OvIFN-τ has been shown to exert its antiproliferative effect *via* slower entry into and prolongation of the S phase of the cell cycle.[7] Twenty-four hours after replating MDBK cells synchronized in G_0/G_1, there are fewer cell remaining in G_0/G_1 and more cells that have progressed to G_2/M in cultures with media alone than observed in the presence of OvIFN-τ (Table 2). Addition of the same peptide, OvIFN-τ(119–150), that primarily reversed OvIFN-τ-induced inhibition of cell proliferation also produced a cell cycle distribution similar to that of media alone, reversing the OvIFN-τ effect. Thus, OvIFN-τ appears to possess multiple functional domains through which different functions may be elicited.

DISCUSSION

Much interest has focused recently on functionally important sites on the IFN-α molecule. Because the related OvIFN-τ protein displays particularly high antiviral and antiproliferative po-

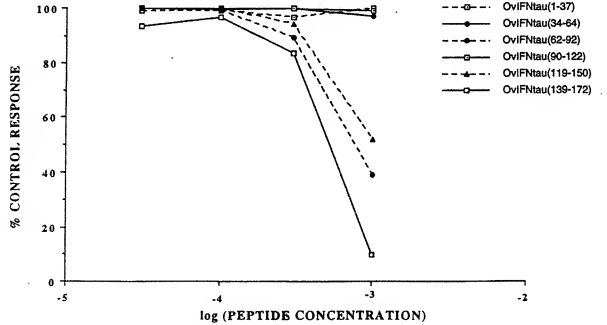

FIG. 4. Peptide inhibition of rBOvIFN-α antiviral activity. Monolayers of MDBK cells were incubated with 40 units/ml rBOvIFN-α in the presence or absence of various concentrations of OvIFN-τ peptides. Results are expressed as the percent of control (without peptide) antiviral activity. Data presented are the means of four replicate experiments. OvIFN-τ(62–92), (119–150), and (139–172) were significantly different from OvIFN-τ(1–37), (34–64), and (90–122) at 10^{-3} *M*. OvIFN-τ(139–172) was significantly different from OvIFN-τ(1–37), (34–64), and (90–122) at 3×10^{-3} *M*. Significance was assessed by analysis of variance followed by Scheffe's F-test at $p < 0.05$.

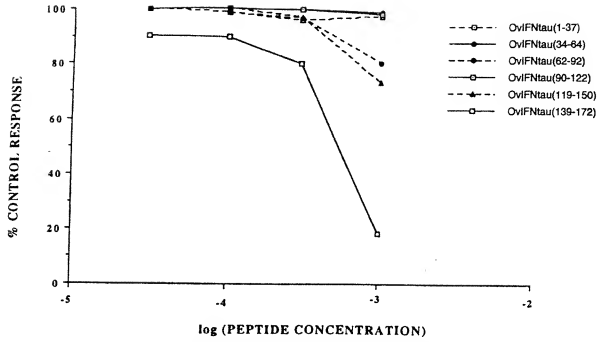

FIG. 5. Peptide inhibition of rHuIFN-α antiviral activity. Monolayers of MDBK cells were incubated with 40 units/ml rHuIFN-α in the presence or absence of various concentrations of OvIFN-τ peptides. Results are expressed as the percent of control (without peptide) antiviral activity. Data presented are the means of three replicate experiments. OvIFN-τ(139–172) was significantly different than all other peptides at all concentrations tested. OvIFN-τ(62–92) and (119–150) were significantly different than all other peptides at 10^{-3} *M*. Significance was assessed by analysis of variance followed by Scheffe's F-test at $p < 0.05$.

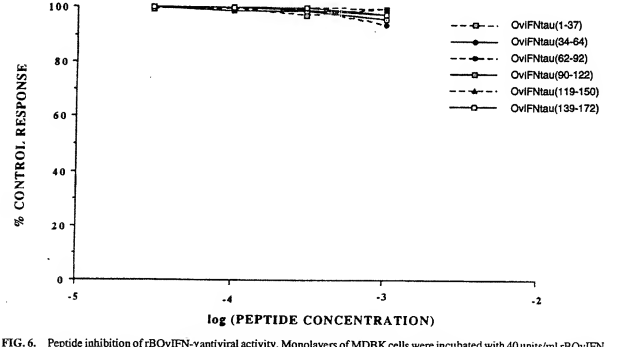

FIG. 6. Peptide inhibition of rBOvIFN-γantiviral activity. Monolayers of MDBK cells were incubated with 40 units/ml rBOvIFN-γ in the presence or absence of various concentrations of OvIFN-τ peptides. Results are expressed as the percent of control (without peptide) antiviral activity. Data presented are the means of three replicate experiments. There were no significant differences among peptides as assessed by analysis of variance followed by Scheffe's F-test at $p < 0.05$.

TABLE 2. PEPTIDE INHIBITION OF OVIFN-τ ANTIPROLIFERATIVE ACTIVITY[a]

Treatment	*Cell number*	G_0/G_1	*S*	*G2/M*[b]
Medium alone	16.7 ± 0	76	13	11
OvIFN-τ	6.9 ± 1.0	79	15	6
OvIFN-τ + OvIFN-τ(1–37)	10.8 ± 1.6	80	14	5
OvIFN-τ + OvIFN-τ(34–64)	9.2 ± 0.3	78	14	5
OvIFN-τ + OvIFN-τ(62–92)	9.4 ± 2.0	79	13	8
OvIFN-τ + OvIFN-τ(90–122)	12.0 ± 1.2[c]	79	15	6
OvIFN-τ + OvIFN-τ(119–150)	16.8 ± 1.5[c,d]	76	13	11
OvIFN-τ + OvIFN-τ(139–172)	12.1 ± 2.2[c]	79	14	6

[a]MDBK cells were cultured at 5–10 × 10^5 cells/well and treated with medium alone, OvIFN-τ at a concentration of 300 units/ml and peptides at 1 m*M*. Cell numbers were determined at 48 h. Duplicate wells were counted in each of three replicate experiments, and the data, normalized by the media control, are expressed as mean cell number × 10^5 ± SE. Cell viability was consistently greater than 95%.

[b]Cell cycle analysis was performed at 24 h. Cells were stained with propidium iodide and analyzed by flow cytometry. Ten thousand cells per sample were examined in replicate experiments, and representative results are expressed as the percentage of cells in each phase of the cell cycle.

[c]Significantly different from OvIFN-τ alone as assessed by analysis of variance followed by Fisher's PLSD ($p < 0.05$).

[d]Significantly different from OvIFN-τ alone as assessed by analysis of variance followed by Scheffe's F-test ($p < 0.05$).

tency concurrently with a lack of cytotoxicity, structural analysis of this molecule to identify functional regions is important. Our initial studies using the amino- and carboxy-terminal synthetic peptides identified the carboxy-terminal region of OvIFN-τ as involved in the antiviral activity by a mechanism and specificity shared by IFNs-α.[8] The involvement of the carboxyl terminus of OvIFN-τ in antiviral function was confirmed in the present study. Furthermore, we have identified additional antiviral regions on OvIFN-τ, specifically amino acids 1–37, 62–92, and 119–150. Although the region of the molecule represented by peptide OvIFN-τ(62–92) has not previously been implicated in functional activity of IFN-τ, an internal region of mouse–human IFN-α hybrid molecules has been implicated in their antiviral activity in bovine cells.[13] Identification of multiple antiviral domains in IFN-τ is consistent with a previous theoretical prediction of IFN-α active sites based on amino acid conservation among various α, β, and ω IFNs.[14] Three conserved clusters were observed: residues 30–39 constituting a predicted external loop, the hydrophilic residues 59–92, and the hydrophobic residues 123–144. Studies of antiviral activity and receptor binding with IFN-α analogs confirmed that three distinct sites, located in the amino-terminal, internal, and carboxy-terminal regions of the molecule, influenced human IFN-α activity.[15] Mutagenesis studies of human IFN-α_4 have indicated amino acids 121–123 and 130–131 in the carboxy-terminal domain,[16,17] and Leu-30, Arg-33, and Phe-36 as critical residues, all of which are conserved in OvIFN-τ.[17,18] Our studies of OvIFN-τ have resulted in identification of multiple sequentially separate regions responsible for antiviral activity for this molecule as well.

Cross-inhibition of IFN-α by the internal and carboxy-terminal peptides suggests that these residues may adopt a similar conformation in both molecules and bind to a common site on the type I IFN receptor. The primary difference between IFN-τ and IFN-α functional domains appears to be within the amino terminus, since the amino-terminal IFN-τ peptide only inhibited OvIFN-τ activity. Thus, this less conserved amino-terminal region of type I IFNs appears to be responsible for the unique functions of IFN-τ, such as potent antiviral activity in the absence of cellular toxicity and antiluteolysis. It follows that the amino terminus of IFN-τ may either have a different affinity for receptor or interact with a different site on the type I IFN receptor than does that of IFN-α.

In contrast to antiviral activity, the antiproliferative activity of IFN-τ was inhibited most effectively by OvIFN-τ(119–150). Since for a particular IFN-α subtype antiviral potency does not necessarily correlate with antiproliferative potency,[19] location of these functions in different domains of the molecule is not unexpected. Within all known IFNs-α, the 8 amino acids between 139 and 147 are highly conserved. These residues are contained in both OvIFN-τ(119–150) and OvIFN-τ(139–172). But while they may be involved in the antiviral activity, they do not appear to be solely responsible for antiproliferative activity because the two peptides were not equivalent inhibitors of OvIFN-τ antiproliferative activity. This observation is consistent with inhibition of antiviral activity, but not antiproliferative activity by a monoclonal antibody to this conserved region in human IFN-α.[20] Another residue, Tyr-123, contained only within OvIFN-τ(119–150), has been found to be necessary for the antiproliferative activity of human IFN-α_1.[21] Nonconservative substitutions at position 123 abrogated antiproliferative function on human and murine cells, and deletion of the residue further eliminated activity on bovine cells. Competition with synthetic peptide would be equivalent to elimination of the interaction between Tyr-123 of OvIFN-τ and the IFN-α receptor on the bovine MDBK cells. It has been reported that mutations around Arg-33 concurrently affected both antiviral and antiproliferative activity of human IFN-α_4 on human cells,[18] but the amino terminus

does not appear to be as important in OvIFN-τ antiproliferative activity on bovine cells. Thus, while OvIFN-τ(119–150) is not the most effective peptide competitor of OvIFN-τ antiviral activity, it can modulate antiproliferative activity. This may result from differential inhibition by individual peptides of OvIFN-τ binding to various regions of the type I IFN receptor. For example, OvIFN-τ(139–172) may interfere preferentially with the interactions of OvIFN-τ with the antiviral site on the receptor. In contrast, OvIFN-τ(119–150) may interfere or block preferentially the interaction of OvIFN-τ with the antiproliferative region of the receptor. The peptides block OvIFN-τ function by blocking the binding to receptor, and they could alter the binding that does occur, resulting in preferential inhibition of particular OvIFN-τ functions.

Given the data on the multiple binding regions of OvIFN-τ, it is important to examine OvIFN-τ secondary and tertiary structure to gain more insight into the structural basis of OvIFN-τ biologic activity. The X-ray crystal structures of IFN-γ and IFN-β have been solved. While IFN-γ exists as a dimer and has low sequence homology to OvIFN-τ, it does fit the common cytokine 4-helix bundle motif.[22] The amino terminus of one monomer is brought into apposition with the carboxyl terminus of the second, and both interact with the IFN-γ receptor. For IFN-β, a loop in the amino terminus is in close proximity to a more carboxy-terminal helix and loop (amino acids 115–138). The amino and carboxyl termini of both IFNs have also been implicated as sites of interaction of the molecules with their respective receptors.[23,24] It has previously been suggested that a third internal helical region of IFN-β is also involved in receptor binding.[25] Structural prediction algorithms and circular dichroism studies of OvIFN-τ secondary structure indicate a primarily α-helical conformation with regions identified as functionally important brought into close proximity (M.A. Jarpe, personal communication). Thus, it appears that OvIFN-τ may fall into a similar structural motif as the other IFNs. Ultimately, determination of the three-dimensional structure of OvIFN-τ, its peptides, as well as the structure of the receptor, will address how these peptides relate to intact OvIFN-τ and how OvIFN-τ interacts with its receptor.

ACKNOWLEDGMENTS

This study was supported by National Institutes of Health grants HD 26006 to H.M.J. and F.W.B., grant CA 38587 to H.M.J., and grant CA 57084 to C.H.P.

REFERENCES

1. BAZER, F.W. (1992). Mediators of maternal recognition of pregnancy in mammals. Proc. Soc. Exp. Biol. Med. **199**, 373–384.
2. IMAKAWA, K., ANTHONY, R.V., KAZEMI, M., MAROTTI, K.R., POLITES, H.G., and ROBERTS, R.M. (1987). Interferon-like sequence of ovine trophoblast protein secreted by embryonic trophectoderm. Nature **330**, 377–379.
3. ROBERTS, R.M., CROSS, J.C., and LEAMAN, D.W. (1992). Interferons as hormones of pregnancy. Endocrine Rev. **13**, 432–452.
4. STEWART, H.J., McCANN, S.H.E., BARKER, P.J., LEE, K.E., LAMMING, G.E., and FLINT, A.P.F. (1987). Interferon sequence homology and receptor binding activity of ovine trophoblast antileucolytic protein. J. Endocrinol. **115**, R13–R15.
5. PONTZER, C.H., TORRES, B.T., VALLET, J.L., BAZER, F.W., and JOHNSON, H.M. (1988). Antiviral activity of the pregnancy recognition hormone ovine trophoblast protein-1. Biochem. Biophys. Res. Commun. **152**, 801–807.
6. BAZER, F.W., JOHNSON, H.M., and YAMAMOTO, J.K. (1989). Effect of ovine trophoblast protein-1 (oTP-1) on replication of feline (FIV) and human (HIV) immunodeficiency viruses. Biol. Reprod. **40** (Suppl. 1), 63 (abstract).
7. PONTZER, C.P., BAZER, F.W., and JOHNSON, H.M. (1991). Antiproliferative activity of a pregnancy recognition hormone, ovine trophoblast protein-1. Cancer Res. **51**, 5304–5307.
8. PONTZER, C.P., OTT, T.L., BAZER, F.W., and JOHNSON, H.M. (1990). Localization of an antiviral site on the pregnancy recognition hormone, ovine trophoblast protein-1. Proc. Natl. Acad. Sci. USA **87**, 5945–5949.
9. OTT, T.L., VAN HEEKE, G., JOHNSON, H.M., and BAZER, F.W. (1991). Cloning and expression in *Saccharomyces cerevisiae* of a synthetic gene for the type-1 trophoblast interferon ovine trophoblast protein-1: Purification and antiviral activity. J. Interferon Res. **11**, 357–364.
10. CHANG, C.D., and MEIENHOFER, J. (1978). Solid-phase peptide synthesis using mild base cleavage of Nα-fluoroenylmethyloxycarbonal amino acids, exemplified by a synthesis of dihydrosomatostatin. Int. J. Peptide Protein Res. **11**, 246–249.
11. FAMILLETTI, P.C., RUBINSTEIN, S., and PESTKA, S. (1981). A convenient and rapid cytopathic effect inhibition assay for interferon. Methods Enzymol. **78**, 387–394.
12. KYTE, J., and DOOLITTLE, R.F. (1982). A simple method for displaying the hydropathic character of a protein. J. Mol. Biol. **157**, 105–132.
13. RAJ, N.B.K., ISRAELI, R., KELLEY, K.A., LEACH, S.J., MINASIAN, E., SIKARIS, K., PARRY, D.A.D., and PITHA, P.M. (1988). Synthesis, antiviral activity, and conformational characterization of mouse-human α-interferon hybrids. J. Biol. Chem. **263**, 8943–8952.
14. ZAV'YALOV, V.P., DENESYUK, A.I., and ZAV'YALOVA, G.A. (1989). Theoretical analysis of conformation and active sites of interferons. Immunol. Lett. **22**, 173–182.
15. FISH, E.N., BANERJEE, K., and STEBBING, N. (1989). The role of three domains in the biological activity of human interferon-α. J. Interferon Res. **9**, 97–114.
16. WEBER, H., VALENZUELA, D., LUJBER, G., GUBLER, M., and WEISSMANN, C. (1987). Single amino acid changes that render human IFN-α2 biologically active on mouse cells. EMBO J. **6**, 591–598.
17. TYMMS, M.J., McINNES, B., WAINE, G.J., CHEETHAM, B.F., and LINNANE, A.W. (1989). Functional significance of amino acid residues within conserved hydrophilic regions in human interferons-α. Antiviral Res. **12**, 37–48.
18. WAINE, G.J., TYMMS, M.J., BRANDT, E.R., CHEETHAM, B.F., and LINNANE, A.W. (1992). Structure-function study of the region encompassing residues 26–40 of human interferon-α_4: Identification of residues important for antiviral and antiproliferative activities. J. Interferon Res. **13**, 42–48.
19. PESTKA, S., LANGER, J.A., ZOON, K.C., and SAMUEL, C.E. (1987). Interferons and their actions. Annu. Rev. Biochem. **56**, 727–777.
20. BARASOAIN, I., PORTOLÈS, A., ARAMBURU, J.F., and ROJO, J.M. (1989). Antibodies against a peptide representative of a conserved region of human IFN-α. Differential effects on the antiviral and antiproliferative effects of IFN. J. Immunol. **143**, 507–512.
21. McINNES, B., CHAMBERS, P.J., CHEETHAM, B.F., BEILHARZ, M.W., and TYMMS, M.J. (1989). Structure-function studies of interferons-α: Amino acid substitutions at the conserved

residue tyrosine 123 in human interferon-α_1. J. Interferon Res. **9**, 305–314.

22. EALICK, S.E., COOK, W.J., VIJAY-KUMAR, S., CARSON, M., NAGABHUSHAN, T.L., TROTTA, P.P., and BUGG, C.E. (1991). Three-dimensional structure of recombinant human interferon-γ. Science **252**, 698–702.
23. SENDA, T., SIMAZU, T., MATSUDA, S., KAWANO, G., SIMIZU, H., NAKAMURA, K.T., and MITSUI, Y. (1992). Three-dimensional crystal structure of recombinant murine interferon-β. EMBO J. **11**, 3193–3201.
24. GRIGGS, N.D., JARPE, M.A., PACE, J.M., RUSSELL, S.W., and JOHNSON, H.M. (1992). The N-terminus and C-terminus of IFNγ are binding domains for cloned soluble IFNγ receptor. J. Immunol. **149**, 517–520.
25. SENDA, T., MATSUDA, D., KURIHARA, H., NAKAMURA, K.T., KAWANO, G., SHIMIZU, H., MIZUNO, H., and MITSUI, Y. (1990). Three-dimensional structure of recombinant murine interferon-beta. Proc. Japan Acad. **66B**, 77–80.

Address reprint requests to:
Dr. Carol H. Pontzer
Department of Microbiology
Building 231
University of Maryland
College Park, MD 20742

Received 10 November 1993/Accepted 11 April 1994

Article No. jmbi.1998.2480 available online at http://www.idealibrary.com on IDEAL J. Mol. Biol. (1999) 286, 151–162

JMB

Exhibit 2

Crystal Structure of Ovine Interferon-τ at 2.1 Å Resolution

Ramaswamy Radhakrishnan[1], Leigh J. Walter[1], Prem S. Subramaniam[3] Howard M. Johnson[3] and Mark R. Walter[1,2]*

[1]*Center for Macromolecular Crystallography and*
[2]*Department of Microbiology University of Alabama at Birmingham, Birmingham AL 35294, USA*

[3]*Department of Microbiology and Cell Science, University of Florida, Gainesville FL 32611, USA*

**Corresponding author*

Ovine interferon-τ (ovIFN-τ) is a pregnancy recognition hormone required for normal embryonic development in sheep. In addition to its novel role in reproductive physiology, ovIFN-τ displays antiviral and antiproliferative activities similar to the IFN-α subtypes. To probe the structural basis for its unique activity profile, the crystal structure of ovIFN-τ has been determined at 2.1 Å resolution. The fold of ovIFN-τ is similar to the previously determined crystal structures of human IFN-α_{2b} and human and murine IFN-β, which each contain five α-helices. Comparison of ovIFN-τ with huIFN-α_{2b}, huIFN-β, and muIFN-β reveals unexpected structural differences that occur in regions of considerable sequence identity. Specifically, main-chain differences up to 11 Å occur for residues in helix A, the AB loop, helix B, and the BC loop. Furthermore, these regions are known to be important for receptor binding and biological activity. Of particular interest, a buried ion pair is observed in ovIFN-τ between Glu71 and Arg145 which displaces a conserved tryptophan residue (Trp77) from the helical bundle core. This ion pair represents a major change in the core of ovIFN-τ compared to huIFN-α_{2b}. Based on amino acid sequence comparisons, these ovIFN-τ structural features may be conserved in several human IFN-α subtypes and IFN-ω. The structure identifies potential problems in interpreting site-directed mutagenesis data on the human IFN-α family that consists of 12 proteins.

Keywords: cytokine; type I interferon; pregnancy hormone; X-ray structure; four-helix bundle

Introduction

Ovine interferon tau (ovIFN-τ) is a member of the type I interferon (IFN) family that also includes IFN-α, IFN-β, and IFN-ω (Roberts *et al.*, 1992). Originally called trophoblast protein-1, ovIFN-τ is the major secretory product of the pre-implanted sheep conceptus during days 13-21 of pregnancy (Godkin *et al.*, 1982). The high level production of ovIFN-τ during this period prevents regression of the corpus luteum (which nourishes the developing embryo) by blocking the pusatile secretion of uterine prostaglandin $F_{2\alpha}$(Roberts, 1991). Despite its novel role in the reproductive physiology of ruminants, ovIFN-τ displays antiviral, antiproliferative, and immunological activities roughly equivalent to IFN-α (Pontzer *et al.*, 1988, 1991).

The mature protein sequences of IFN-τ, as well as IFN-ω, contain 172 amino acid residues compared to 166 for IFN-α subtypes (165 for IFN-α_2) and IFN-β (Imakawa *et al.*, 1987). The six additional residues of IFN-τ and IFN-ω are located at the C terminus of the molecule. OvIFN-τ shares amino acid sequence identities of approximately 50% with human IFN-α and IFN-ω sequences, and 30% with human IFN-β. The three-dimensional type I IFN fold has been elucidated by crystal structures of human IFN-α_{2b}, and murine and human IFN-β (Radhakrishnan *et al.*, 1996; Senda *et al.*, 1995a; Karpusas *et al.*, 1997). The IFNs are members of the α-helical cytokine family which adopt a common four-helix bundle topology first observed for porcine growth hormone (Abdel-

Abbreviations used: cm, calculated mass; hu, human; IFN, interferon; MALDI, matrix assisted laser desorption/ionization; mu, murine; ov, ovine; TOF, time of flight.

E-mail address of the corresponding author: walter@onyx.cmc.uab.edu

0022-2836/99/060151–12 $30.00/0

Meguid *et al.*, 1987). The type I IFN fold is distinguished from other α-helical cytokines by the presence of a fifth helix which tightly associates with the helix bundle (Sprang & Bazan, 1993).

Cellular responses to the human type I IFNs require at least two receptor chains, IFNAR-1 and IFNAR-2 (Uzé *et al.*, 1990; Domanski *et al.*, 1995). The extracellular domain of the IFNAR-2 adopts a modular architecture consisting of tandem fibronectin type III domains (Seto *et al.*, 1995). The interface between these domains is proposed to form the IFN binding site. The IFNAR-1 chain contains four fibronectin type III domains and may bind two IFNs simultaneously. The intracellular domains of IFNAR-1 and IFNAR-2 are associated with Tyk-2 and Jak-1 kinases, respectively (Barbieri *et al.*, 1994; Colamonici *et al.*, 1996). Cell signaling is thought to occur by IFN-induced receptor oligomerization. This activates the intracellular kinases and subsequently nuclear transcription activators (STATS) that stimulate the appropriate biological responses (Pellegrini & Dusanter-Fourt, 1997). Recently, the antiproliferative activities of IFN-α on T-cells have been shown to require components of the T-cell receptor signaling pathway CD45, Lck, and ZAP-70 (Petricoin *et al.*, 1997).

Increasing evidence suggests that the different activity profiles of the IFNs are due to altered affinities for their receptors. The unique activity profile of ovIFN-τ makes it an excellent candidate for studying type I IFN receptor-ligand interactions. For example, IFN-τ and IFN-α share equivalent antiviral activities, yet IFN-α is much less effective in sustaining the lifespan of the corpus luteum (Roberts *et al.*, 1991). Additional studies have shown that unlike IFN-α, ovIFN-τ is less toxic to cells when administered *in vitro* at high concentrations (Pontzer *et al.*, 1991; Subramaniam *et al.*, 1995; Strander, 1989). Furthermore, synthetic ovIFN-τ peptides 1-37, 62-92, 119-150, and 139-172 inhibit ovIFN-τ antiviral activity on MDBK cells in a dose dependent manner (Pontzer *et al.*, 1990, 1994). However, only peptides 62-92, 119-150, and 139-172 inhibited human IFN-α antiviral activity. These data suggest that differences in receptor binding and biological activity between ovIFN-τ and human IFN-α are localized to the N terminus of the molecules. Understanding the detailed structural mechanisms of IFN receptor engagement is important, since the human type I IFNs have been shown to be effective in the treatment of approximately 15 diseases worldwide, including hairy-cell leukemia, hepatitis, Kaposi's sarcoma, and multiple sclerosis (Baron *et al.*, 1991; Nagabhushan & Giaquinto, 1995).

Based on the high degree of sequence identities of the type I IFNs, homology models of IFN-τ have been constructed using the structure of murine IFN-β (Jarpe *et al.*, 1994; Senda *et al.*, 1995a,b). Here, we report the crystallization and structure determination of ovIFN-τ at 2.1 Å resolution. Differences in receptor binding and biological activity of ovIFN-τ and IFN-α_{2b} may be correlated with the structural deviations observed in helices A, B, and E, as well as the AB and BC loops. Based on amino acid sequence analysis of the human IFN-α subtypes, structural features observed in ovIFN-τ may also be found in a subset of the human IFN-α subtypes. The structure also identifies potential problems in interpreting site-directed mutagenesis data on the human IFN-α family that consists of 12 proteins.

Results

Quality of the structure

The crystal structure of ovIFN-τ was solved by multiple isomorphous replacement and refined to 2.1 Å resolution. Molecular replacement (MR) studies using AMoRe (Navaza, 1994) with human IFN-α_{2b}, murine IFN-β, and other helical cytokines as the search models were unsuccessful. However, since ovIFN-τ contains an unpaired cysteine residue at position 86, mercury derivatives were easily identified (Table 1). The final *R*-factor for all data between 15-2.1 Å is 21.4% with a free *R*-factor of 25.0% (Table 2). Root-mean-square deviations from ideal bond lengths and angles are 0.01 Å and 1.4°, respectively. All residues have main-chain dihedral angles in allowable regions of ϕ/ψ space with 90.0% in the most favored region (Figure 1). The final model consists of residues 1-101 and 114-164, two sulfate ions, and 87 water molecules. The side-chains of Asp115, Gln125, and Arg161 are modeled as alanine residues. The diffraction pat-

Table 1. Heavy-atom data statistics

Data set	Resolution (Å)	Reflections Measured	Reflections Unique	Completeness (%)	R_{sym}[a] (%)	MIFD[b] (%)	Phasing[c] power	R_{cullis}[d]
Native	2.7	18,740	4246	99.0	6.1			
$HgAc_2$	2.8	16,752	3801	99.0	6.6	27.0	1.94	0.67
EMTS	3.4	8994	2163	97.4	8.2	18.6	1.72	0.68
K_2PtCl_4	3.8	5056	1487	92.5	7.2	21.6	0.80	0.91
$K_2Pt(NO_2)_4$	3.8	8564	1573	97.0	8.8	21.1	0.70	0.92

[a] $R_{sym} = \Sigma|I_d - \langle I_d \rangle|/\Sigma I_d$, where $\langle I_d \rangle$ is the average over multiple observations.
[b] MIFD = Mean Isomorphous Difference, $\Sigma|F_{PH} - F_P|/\Sigma F_{PH}$ where F_{PH} and F_P are the derivative and native structure factor amplitudes, respectively.
[c] Phasing power = $|F_{H(calc)}|/||F_{PH(obs)} - F_{PH(calc)}||$.
[d] $R_{cullis} = \Sigma||F_{PH(obs)} \pm F_{P(obs)}| - F_{H(calc)}|/\Sigma|F_{PH(obs)} - F_{P(obs)}|$.

Table 2. Refinement statistics

A. Data	
Resolution (Å)	15-2.1
No. of reflections/unique	85,769/8216
Completeness (%)	96.9
R_{sym}	0.043
B. Model	
No. protein atoms	1237
No. solvent molecules	87 H_2O, 2 SO_4
Average *B*-factor (protein 1, H_2O); (Å²)	39.4/47.7
R_{cryst}, 15.0-2.1 Å	21.4
R_{free}, 15.0-2.1 Å	25.0
rmsd bonds (Å)	0.01
rmsd angles (deg.)	1.4
rmsd *B*-factor (bonded atoms; Å²)	1.9

terns of ovIFN-τ exhibit significant thermal diffuse scattering that is consistent with a highly mobile protein structure. Analysis of the electron density and individual *B*-factors shows that this flexibility is mainly located in the loop regions of ovIFN-τ. Representative electron density for residues in the core of the molecule and the loop regions are shown in Figure 2(a) and (b).

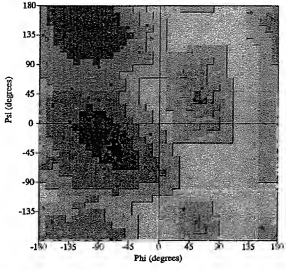

Figure 1. Ramachandran plot of the refined model of ovIFN-τ. The Figure was generated with the program Procheck (Laskowski *et al.*, 1993).

Structure of ovIFN-τ

OvIFN-τ is a monomer with overall dimensions of 20 Å × 30 Å × 40 Å (Figure 3). The molecule adopts a type I interferon fold that contains five α-helices (labeled A-E) which are linked by one overhand loop (Presnell & Cohen, 1989) the AB loop, and three shorter segments (BC, CD, and DE loops). Helices A, B, C, and E are antiparallel and tightly associated to form a left-handed four-helix bundle. Helix D runs approximately parallel with helix B and together with the extended portion of the AB loop packs against helices B and E. All five helices are relatively straight, with the exception of helix E that contains a 20° bend centered at Met148. This bend allows helix E to maximize its packing contacts with the rest of the helix bundle. The hydrophobic core of the molecule is predominantly made up of leucine residues. Several polar residues (Asn14, Ser64, Glu71, Gln92, Tyr123, Arg145, Ser155, Thr156, and Gln159) are buried in the molecular core. Five of these residues (Asn14, Gln92, Ser155, Thr156, and Gln159) form an extensive hydrogen bond network that includes two buried water molecules (Figure 2(a)).

The AB loop connects helix A and B. It is best described in three segments labeled the AB1 (residues 25-33), AB2 (residues 34-39), and AB3 (residues 40-52) loops. The BC, CD, and DE loops are made up of residues 75-79, 101-115, and 134-137, respectively. The AB1 loop is linked to helix E through a disulfide bond between Cys29 and Cys139. The AB2 loop runs parallel with the helix bundle and contributes Phe36 and Leu38 to the hydrophobic core of the molecule. Residues on the exposed surface of the loop form two stabilizing interactions. First, $O^{\delta1}$ of Asp35 forms a hydrogen bond with the nitrogen atom of Gly37. Second, the main-chain oxygen of Leu38 forms a hydrogen bond with the $N^{\varepsilon2}$ atom of Gln40. The BC loop forms a solvent-accessible β-turn that places Trp77 away from the interior of the molecule. In the crystal, Trp77 packs into a hydrophobic pocket between helices A, C, and D of a symmetry related molecule (Figure 4). The hydrophobic pocket is formed by amino acid residues Cys1, Leu7, Phe54, Leu57, Leu96, Cys99, and Leu162. In other type I IFN structures, Trp77 packs into the hydrophobic core of the molecule near Trp141. The location of Trp77 in IFN-α_{2a}, as well as human and murine IFN-β is replaced by Glu71 in ovIFN-τ. The negatively charged glutamic acid residue forms a buried ion pair with Arg145. The high *B*-factors (~65 Å²) observed for the BC loop suggest that it can adopt multiple conformations in solution. A notable feature of the DE loop is the left-handed α-helical conformations of Gly135 and Tyr136. This distinct loop structure places the O^{γ} atom of Ser137 in position to form a bifurcated hydrogen bond with the N atoms of Cys139 and Ala140 that form the first turn of helix E.

Although electron density is observed for the AB1, AB3, and BC loops, these loop regions have high *B*-factors and are presumed to adopt multiple conformations in solution. Each of these flexible residue segments are solvent exposed and found at the ends of the more rigid helix bundle. No electron density is observed for residues 102-113, and 165-172 located in the CD loop and C terminus, respectively. Analysis of ovIFN-τ crystals by MALDI-TOF mass spectroscopy revealed two broad peaks at 12,664.0 and 7255.5. These peaks likely correspond to ovIFN-τ peptide fragments 1-109 (calculated mass (cm) = 12,699) and 110-174 (cm = 7233.3), and suggest that the protein is being

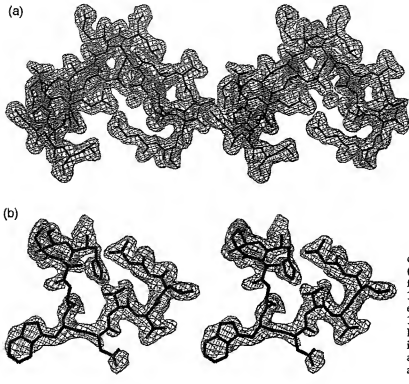

Figure 2. Stereoviews of the final ovIFN-τ electron density maps. (a) Final $2F_o - F_c$ electron density for helical residues 10-15, 89-96, 152-159 and two buried water molecules. The density is contoured at 1.0σ. (b) Final $2F_o - F_c$ density for BC loop residues 72-82. The density is contoured at 0.75σ. Carbon atoms are shown in green, oxygen in red, and nitrogen in blue.

cleaved in the CD loop between Asp109 and Ser110 during the extended crystallization experiment (six weeks). Additional cut sites in the CD loop are predicted from the identification of additional peaks that correspond to the ovIFN-τ fragments 1-106/107-172 and 1-112/113-172. Interestingly, mass spectroscopy on fresh crystallization drops revealed two peaks of 19,992.0 and 20,076.0 which corresponds to ovIFN-τ (cm = 19,914.5) plus one (cm = 19,994.5) or two (cm = 20,074.5) sulfate ions. This data provides a plausible reason for the lack of electron density for residues in the CD loop and also strengthens our interpretation of two large density peaks as sulfate ions. Adjacent to the disordered C terminus, well-defined electron density is observed for the N terminus of the molecule.

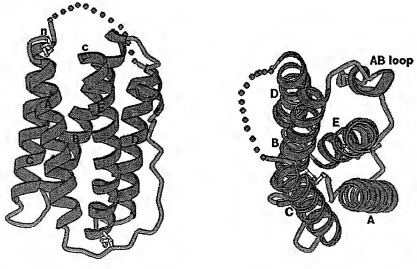

Figure 3. Ribbon diagram of ovIFN-τ. Two views are shown at 90° to one another. Helices are colored cyan and loops yellow. The CD loop not observed in the electron density map is denoted with red spheres for clarity.

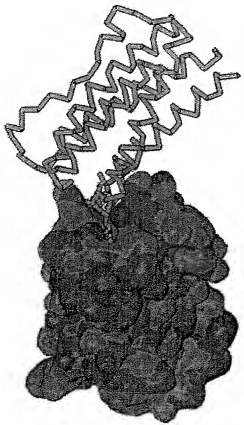

Figure 4. Crystal packing environment of Trp77. One ovIFN-τ molecule is represented as an accessible surface. Surface accessible carbon, oxygen, and nitrogen atoms are represented by green, red, and blue surfaces, respectively. A symmetry-related ovIFN-τ molecule is represented by C^{α} atoms. All atoms are shown for residues 75-80 of this molecule.

A second disulfide is found between Cys1 and Cys99 and links the N terminus to helix C. The fifth unpaired cysteine residue in ovIFN-τ (Cys86) is located on helix C where it is partially buried in the core of the molecule.

Conserved structural core of the type I IFNs

The overall fold of ovIFN-τ and IFN-α_{2b} are similar; 141 C^{α} atoms can be superimposed with a root-mean-square difference (rmsd) of 2.9 Å (Figure 5). Outliers in the superposition, C^{α} atoms that differ by more than 3 Å, are residues 6-7 at the N terminus, 23-32 in helix A and the AB1 loop, 49-52 in the AB3 loop, 71-77 in helix B and the BC loop, and 158-159 in helix E. The rmsd for the remaining 111 residue pairs is 1.2 Å. The C^{α} atom comparisons between ovIFN-τ and human and murine IFN-β yield overall rmsd values of ~3 Å for 140 residue pairs. Excluding C^{α} atom outliers greater that 3 Å results in a rmsd of ~1.3 Å for 114 atom pairs. The comparisons reveal a common conserved structural core (C^{α} differences less than 2 Å) between ovIFN-τ, huIFN-α_{2b}, huIFN-β, and muIFN-β, which consists of helix A (residues 8-21), AB2 loop (residues 34-39), helix B (residues 53-68), helix C (residues 79-100), and helices D and E (residues 117-155).

Comparison with IFN-α_{2b}

Helix A is eight residues longer in ovIFN-τ (residues 4-24) than in IFN-α_{2b} (residues 9-21). The C-terminal extension of helix A in ovIFN-τ, results in C^{α} atom differences of more than 6 Å for residues 23-25 (Figure 6). These structural changes result in new side-chain hydrogen bonds between $O^{\delta1}$ and $N^{\delta2}$ atoms of Asn22 with the O and NH1 atoms of Arg145 and between the O^{γ} of Ser25 with the $O^{\epsilon2}$ atom of Glu142. Relative to IFN-α_{2b}, the side-chain of Arg145 moves 5 Å towards the interior of the molecule. Additional differences in side-chain positions between ovIFN-τ and IFN-α_{2b} occur for Arg23 (~16 Å) and Leu24 (~11 Å). These large movements reflect the reverse orientations of Arg23 and Leu24 which point at the BC loop in IFN-α_{2b} and into the solvent near helix A in ovIFN-τ. Extension of helix A shortens the AB1 loop by two residues in ovIFN-τ and leads to main-chain differences with IFN-α_{2b} of up to 11 Å.

Additional differences of about 6 Å occur in helix B. Helix B is straight in ovIFN-τ and exhibits a 70° kink in IFN-α_{2b}. Four residues in IFN-α_{2b} (Ser69, Lys71, Asp72, and Tyr86) and ovIFN-τ (Tyr69, Glu71, His72, and Cys86) participate in different interactions that stabilize helix B in the kinked or straight conformation (Figure 7). The α-helical hydrogen bond pattern is disrupted by the kink in helix B of IFN-α_{2b}. Substitute hydrogen bonds to the exposed carbonyl oxygen atoms of helix B are formed by the side-chains of Ser69 and Tyr86. The position of the bulky Tyr86 side-chain in IFN-α_{2b} provides an additional steric constraint that promotes the kink in helix B. Tyrosine 69 and Cys86 in ovIFN-τ remove the hydrogen bonding and steric constraints provided by Ser69 and Tyr86 in huIFN-α_{2b}. An additional hydrogen bond is formed in ovIFN-τ between His72 of helix B and Glu83 on helix C.

The kink in helix B allows the BC loop of IFN-α_{2b} to pack tightly against the end of the helix bundle, while the straight extension of helix B observed in ovIFN-τ extends the BC loop away from the molecule. These differences significantly change the accessibility of residues located on helix B and the BC loop. In particular, the C^{α} position of Trp77 moves by 8.5 Å and does not pack against Trp141 in the interior of the protein as found for IFN-α_{2b} (Radhakrishnan *et al.*, 1996). The side-chain location of Trp77 in huIFN-α_{2b} is replaced by Glu71 in ovIFN-τ where it forms a buried salt bridge with Arg145. The buried environment of Glu71 in ovIFN-τ, was unexpected, since Lys71 is fully solvent exposed in huIFN-α_{2b} (Figure 7). The

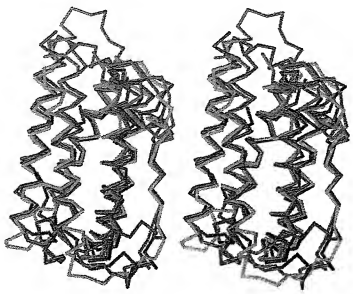

Figure 5. Stereoview comparison of the type 1 interferon structures. Only C^{α} atoms of ovIFN-τ (gold), huIFN-α_{2b} (green), huIFN-β (red), and muIFN-β (cyan) are shown.

distance between the C^{α} atom of Glu71 in ovIFN-τ and Lys71 in huIFN-α_{2b} is about 6 Å.

The conformation of helix B (straight or kinked) depends on the amino acid residues found at positions 69, 71, 72, and 86. Besides other ovIFN-τ sequences, the ovIFN-τ residue pattern (Tyr69, Glu71, His72, Cys86) is not strictly conserved in the type I IFN sequences (Figure 8). On the other hand, the residue pattern found in huIFN-α_{2a} (Ser69, Lys71, Asp 72, Tyr86) is observed in human subtypes IFN-α_2, IFN-α_5, IFN-α_6, IFN-α_8, and IFN-α_{16}. Interestingly, a subset of human IFN-α subtypes IFN-α_4, IFN-α_7, IFN-α_C, and IFN-α_{17} have a Glu at position 71 and a Ser rather than Cys at position 86 as observed in ovIFN-τ. For huIFN-ω (His69, Glu71, Arg72, His86), only Glu71 is conserved with ovIFN-τ.

Structural differences between ovIFN-τ and huIFN-α_{2b} at the C-terminal end of helix E reflect the 20° bend which is found in helix E of ovIFN-τ, but not in huIFN-α_{2b}. The structural differences in helix E are influenced by Ser151 which, along with Glu147, forms a bifurcated hydrogen bond with Tyr123 in huIFN-α_{2b} (Radhakrishnan *et al.*, 1996). In ovIFN-τ, Ser151 is replaced by an alanine. Consistent with the Ser → Ala substitution, helix E in ovIFN-τ rotates clockwise ~20° (looking down the helix axis from the C terminus) which packs the methyl group of the alanine into the hydrophobic core of the molecule. Despite the rotation, C^{α} atom differences greater than 3 Å do not occur until residues 158-159. In this region of ovIFN-τ, hydrogen bonds are formed between the $O^{\varepsilon 1}$ and $N^{\varepsilon 2}$ of Gln 159 with the $N^{\varepsilon 2}$ of Gln92 and the O of Leu7 (Figure 2(a)). These interactions are not observed in huIFN-α_{2b}. Helix E is three amino acid residues longer in ovIFN-τ compared to helix E in huIFN-α_{2b}. Residues following Lys164 in ovIFN-τ and Glu160 in huIFN-α_{2b} are not observed and presumed to be flexible.

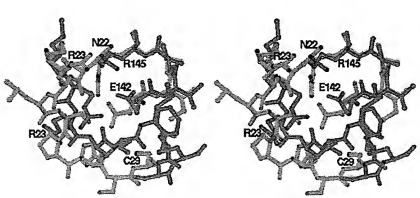

Figure 6. Stereoview comparison of helix A and the AB1 loop between ovIFN-τ (gold) and huIFN-α_{2b} (cyan). Residues 21-29 and 142-145 are shown. Oxygen and nitrogen atoms are colored red and blue, respectively. Selected residues are labeled.

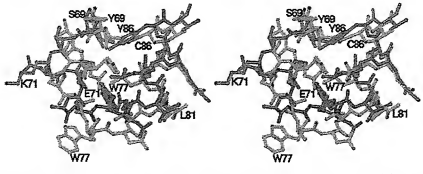

Figure 7. Stereoview comparison of helix B and the BC loop between ovIFN-τ (gold) and huIFN-α_{2b} (cyan). Residues 67-87 are shown. Oxygen and nitrogen atoms are colored red and blue, respectively. For clarity, the side-chains of residues 67, 68, and 85 have been removed from the Figure. Selected residues are labeled.

Discussion

In contrast to the zinc mediated dimers observed for human IFN-α_{2b} (Radhakrishnan *et al.*, 1996) and IFN-β (Karpusas *et al.*, 1997), ovIFN-τ is a monomer in the crystal. Superposition of ovIFN-τ, huIFN-α_{2b}, huIFN-β, and muIFN-β monomers, which display 30-50% sequence identity, reveals a conserved structural core of five α-helices and the AB2 loop. Regions that display the largest structural variations are also conserved. The greatest differences in C^{α} atom positions (~6-11 Å) occur in helix A, the AB1 loop, helix B, and the BC loop. These structurally variable regions are located on one end of the helix bundle where they likely play a significant role in the different functional properties of all type I IFNs. The structural differences in the loops are controlled by differences in the lengths and packing of the helices with few interactions within the middle of the loops. Furthermore, the hydrogen bond network between Asn22 (helix A), Arg145 (helix E) and Glu71 (helix B) provides a structural mechanism by which receptor binding at the AB1 loop may result in conformational changes to the BC loop.

OvIFN-τ and huIFN-α_2 compete for the same receptors on human and bovine cells and are predicted to share similar receptor binding sites (Subramaniam *et al.*, 1995; Li & Roberts, 1994a). The observed structural differences in helix A and the AB loop between ovIFN-τ and huIFN-α_{2b} (residues 1-8 and 22-32) occur in regions implicated in the differential receptor recognition and/or biological activity of ovIFN-τ and IFN-α_2. Specifically, hybrid scanning studies have shown that sequence differences within residues 16-28 are responsible for ~50-fold differences in activity between huIFN-α_1 and huIFN-α_2 on human cells (Weber *et al.*, 1987). Furthermore, an ovIFN-τ synthetic peptide (residues 1-37) was found to inhibit the antiviral activity of ovIFN-τ, but not huIFN-α_2, on MDBK cells (Pontzer *et al.*, 1994).

Despite the significant structural changes in helix B and the BC loop (residues 71-79) between ovIFN-τ and huIFN-α_{2b}, mutational analysis has mostly identified the exposed residues of helix C (residues 80, 84, 86, and 90) in receptor binding and altered biological activity (Uzé *et al.*, 1994). This apparent discrepancy may be explained by the unique hydrogen-bonding networks observed in the straight (ovIFN-τ) or kinked (huIFN-α_{2b}) conformation of helix B. In particular, Tyr86 participates in important Van der Waal's and hydrogen bond interactions that stabilize helix B in the bent conformation in IFN-α_{2b}. A similar structural role for tyrosine residues has been observed in the bent helices of the related cytokines IL-10 and IFN-γ (Walter & Nagabhushan, 1995). Hybrid studies have shown that sequence differences between IFN-α_1 and IFN-α_2 at positions Ser69 → Thr, Thr 80 → Asp, and Tyr86 → Cys cause a reduction of IFN-α_2 activity on human cells, while simultaneously increasing its activity on murine cells (Rehberg *et al.*, 1982). Substitution of Tyr86 with Cys is required to obtain the straight helix B and flexible BC loop observed in ovIFN-τ. Thus, the Tyr86 → Cys substitution on helix C in the IFN-α chimera may also result in conformational changes to residues 71-79.

The presence of Glu71 and Ser86 in the human IFN-α_4, IFN-α_7, IFN-α_C and IFN-α_{17} suggests that these four human subtypes adopt an extended helix B and BC loop conformation similar to ovIFN-τ. Additional non-conservative amino acid residue differences between the four subtypes and IFN-α_{2b} occur in helix A and helix E. Each residue is located in helices that display significant structural differences in ovIFN-τ and huIFN-α_{2b}. For huIFN-α_{2b}, Arg22 is replaced by Gly22 in each of the four subtypes. Furthermore, residue position 160 is a Glu in huIFN-α_{2b} and a Lys in ovIFN-τ, IFN-α_4, IFN-α_7, IFN-α_C and IFN-α_{17}. Neither Glu160 in huIFN-α_{2b} nor Lys160 in ovIFN-τ plays a role in stabilizing the conformation of helix E. Consistent with the predicted similarities of ovIFN-τ and huIFN-α_4, deletion of 11 residues from the C terminus of ovIFN-τ or eight residues from the C terminus of IFN-α_4 reduces antiviral activity to a greater extent than removing 11 resi-

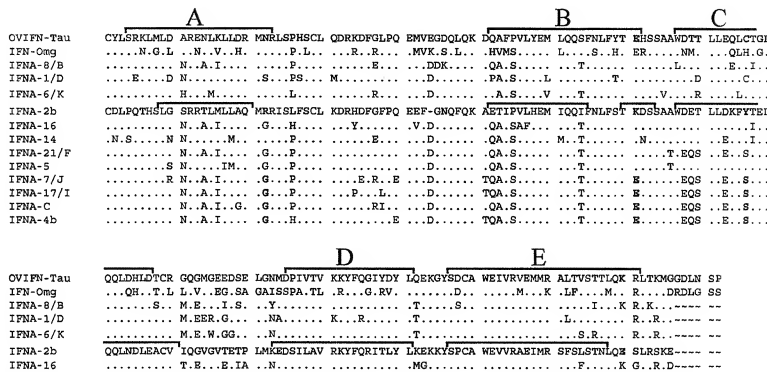

Figure 8. Amino acid sequence alignment of ovIFN-τ, huIFN-ω, and the 12 human IFN-α subtypes (Pestka, 1997). Residues are shown in blocks of ten. The location of the α-helices for ovIFN-τ and huIFN-α_{2b} are shown as black bars. All residues are shown for ovIFN-τ and huIFN-α_{2b}. For other sequences, a period is shown for residues with sequence identity to huIFN-α_{2b}. Residues 22, 71, 86, and 160 that were identified as markers of the structural differences between ovIFN-τ and huIFN-α_{2b} and are conserved among human IFN-α subtypes α_{5}, α_{17}, α_{c} and α_{4b} are in bold type.

dues from the C terminus of IFN-α_2 (Li & Roberts, 1994b; Cheetham *et al.*, 1991; Chang *et al.*, 1983).

The IFNAR-2 has been shown to bind several human IFN-α subtypes as well as IFN-β, while the IFNAR-1, although required for biological activity, plays only a complementary role in ligand binding affinity (Cohen *et al.*, 1995). Structure-function studies with human IFN-α suggest that the IFNAR-1 binding site is made up of exposed residues on helix A and C (Uzé *et al.*, 1994). On the opposite side of the molecule, the IFNAR-2 binding site is predicted to consist of a group of highly conserved residues on the AB loop, helix D, and the DE loop (Mitsui *et al.*, 1993). Despite crystal structures for growth hormone and IFN-γ receptor complexes (de Vos *et al.*, 1991; Walter *et al.*, 1995), attempts to construct a plausible IFN-α receptor complex model that explains all of the structure-function data has not been accomplished. This may reflect yet unidentified interactions between the type I IFNs and their receptors, or be the result of misinterpreting the structural consequences of various mutational data. The complexities of interpreting structure-function data in the type I IFN system arise from the potential biological importance of IFN-α and IFN-β dimers (Radhakrishnan *et al.*, 1996; Karpusas *et al.*, 1997), novel splice variants for the IFNAR-1 (Cook *et al.*, 1996), and the recent identification of at least one additional receptor chain on human T cells (Petricoin *et al.*, 1997).

The crystal structure of ovIFN-τ provides information on the conformational variability of the type I IFNs. The location of structurally conserved and variable regions between ovIFN-τ and huIFN-α_{2b} is consistent with the functional properties and proposed binding sites of the known IFN-α receptors. For example, the requirement of the IFNAR-2 to bind a common site on all type I IFNs is supported by the low rmsd (0.4 Å, residues 34-41 and 115-149) between ovIFN-τ and huIFN-α_{2b} in the proposed IFNAR-2 binding site. In contrast, larger structural changes (0.8 Å, residues 8-22 and 80-100) are observed between ovIFN-τ and huIFN-α_{2b} in helix A, which along with helix C is proposed to interact with the signal transducing IFNAR-1. The large structural differences between ovIFN-τ and huIFN-α_{2b} in helix B and the BC loop suggest that they are important for receptor binding, although little biochemical evidence is currently available in the human IFN-α system. The structural differences in this region may be involved in the unique function of ovIFN-τ as a pregnancy recognition hormone. The close proximity of helix B and the BC loop to helix C suggests that it could also form part of the IFNAR-1 binding site. Additional mutagenesis studies with purified receptor components as well as a crystal structure of a type I IFN receptor complex will be required to answer these questions.

Materials and Methods

Crystallization

Recombinant ovIFN-τ was expressed in yeast (*Pichia pastoris*) and purified as described (Ott *et al.*, 1991). The purified protein was crystallized by hanging-drop vapor diffusion techniques. The protein drops consisted of 1 μl of ovIFN-τ solution (20 mg/ml) and 1 μl of the reservoir solution consisting of 0.8 M $LiSO_4$, 100 mM citrate buffer (pH 4.8). The drops were equilibrated over 1 ml of reservoir solution at room temperature. Crystals, with maximum dimensions of 0.35 mm^3, were obtained after about six weeks. The crystals belong to the orthorhombic space group $P2_12_12_1$ with unit cell dimensions of $a = 39.30$ Å, $b = 45.60$ Å, and $c = 75.84$ Å. The crystals contain one molecule in the asymmetric unit which corresponds to a solvent content of about 27% (Matthews, 1968). Mass analysis of ovIFN-τ crystals was carried out on a Voyager Elite mass spectrometer with delayed extraction technology (PerSeptive Biosystems, Framingham, MA) operating in the positive mode. The acceleration voltage was set at 25 kV and 50-100 laser shots were summed. Samples were mixed 1:10 with Sinapinic acid dissolved in acetonitrile:0.1% (v/v) trifluoroacetic acid (1:1). Apomyoglobin was used as an internal standard.

X-ray data collection and MIR phasing

Intensity data were collected using a R-AXIS IV image plate detector using CuKα radiation ($\lambda = 1.5418$ Å) from a Rigaku RU-200 rotating anode generator (50 kV, 100 mA) equipped with focusing mirrors (MSC, The Woodlands, Texas). Initial native and heavy-atom derivative datasets were collected at room temperature (Table 1). A final native dataset was collected at −170°C (Table 2). Crystals were prepared for low temperature data collection by equilibration in a cryoprotectant solution containing 20% (v/v) glycerol, 1.4 M $LiSO_4$, and 100 mM citrate buffer (pH 4.8). Data were integrated and scaled using the programs DENZO and SCALEPACK (Otwinowski, 1993). All multiple isomorphous replacement calculations were performed using the CCP4 suite of programs (CCP4, 1994). The single site $HgAc_2$ and EMTS derivatives were identified by inspection of difference Patterson maps. Two additional weak derivatives (K_2PtCl_4 and $K_2Pt(NO_2)_4$) were identified by mercury cross-phased difference Fourier maps. Despite their poor statistics, maps calculated with these two additional derivatives were of better quality than the two derivative maps. Heavy-atom refinement and subsequent phase calculations were carried out in MLPHARE (Table 1; Otwinowski, 1991). MIR phases were calculated at 2.8 Å and anomalous data were included for the $HgAc_2$ derivative. The phases were further improved by solvent leveling and histogram matching procedures in DM (Cowtan, 1994). The resulting DM modified electron density map displayed well-defined α-helices corresponding to residues 4-23, 56-72, 81-99, and 122-160. Alignment of the sequence to the map was facilitated by the model of recombinant human IFN-α_{2b} (PDB entry 1RH2). Model building was done using the interactive graphics programs TOM (Cambillau & Horjales, 1987) and O (Jones & Kjeldgaard, 1993). Confidence in the sequence alignment was obtained by the overall agreement of the side-chain electron density for each ovIFN-τ residue. In addition, the heavy-atom sites were located close to ovIFN-τ side-chains that had affinity for that particular metal ion.

Structure refinement

Initial refinements were done using X-PLOR 3.8.5 (Brunger, 1991) using the stereochemical parameter files defined by Engh & Huber (1991). Prior to refinement, 10% of the data were randomly omitted for monitoring the free *R*-factor (Brunger, 1992). The initial model was subjected to four cycles of simulated annealing using X-PLOR, SIGMAA weighting, and phase combination (Read, 1986) which resulted in an R_{free} of 31.9%. Additional torsion angle dynamic refinement (Rice & Brunger, 1997) was carried out using the maximum likelihood target function (Pannu & Read, 1996) as implemented in CNS (Brunger *et al.*, 1998). CNS refinements included corrections for the bulk solvent and anisotropy in the diffraction data (Jiang & Brunger, 1994). The stereochemical quality of the ovIFN-τ model at all stages in the refinement was monitored using PROCHECK (Laskowski *et al.*, 1993). Model superpositions were performed manually using the computer graphics and improved by least squares (Kabsch, 1976). Amino acid sequence alignments were performed using the GCG computer package (Wisconsin Package Version 9.0). For comparison, residues in ovIFN-τ and IFN-α_{2b} were numbered according to the consensus IFN sequence which counts the deletion at position 44. The graphics program CHAIN was used to generate Figure 2 (Sack, 1988). The RIBBONS program suite was used to generate Figures 3-7 (Carson, 1991)

Protein Data Bank accession number

OvIFN-τ coordinates and structure factors have been deposited in the Brookhaven Protein Data Bank accession nos 1b51 and 1b51sb.

Acknowledgments

We thank Maxine Rice and Jun Dai for help in manuscript preparation, and Lori Coward in the UAB Comprehensive Cancer Center for MALDI-TOF mass spectroscopy. This work was supported in part by grants to M.R.W. from the American Heart Association (Grant no. 96008020) and the NIH (Grant no. AI36871), and to H.M.J. through NIH grant no. CA69959.

References

Abdel-Meguid, S. S., Shieh, H.-S., Smith, W. W., Dayringer, H. E., Violand, B. N. & Bentle, L. A. (1987). Three-dimensional structure of a genetically engineered variant of porcine growth hormone. *Proc. Natl Acad. Sci. USA*, 84, 6434-6437.

Barbieri, G., Velazquez, L., Scrobogna, M., Fellous, M. & Pellegrin, S. (1994). Activation of the protein tyrosine kinase tyk2 by interferon α/β. *Eur. J. Biochem.* 232, 427-435.

Baron, S., Tyring, S. K., Fleischmann, W. R., Coppenhaver, D. H., Neisel, D. W., Klimpel, G. R., Stanton, G. J. & Hughes, T. K. (1991). Mechanisms of action and clinical applications. *J. Am. Med. Assoc.* 266(10), 1375-1383.

Brunger, A. T. (1991). *X-PLOR, Manual Version 3.1*, Yale University Press, New Haven, CT.

Brunger, A. T. (1992). Free R value: a novel statistical quantity for assessing the accuracy of crystal structures. *Nature*, 355, 472-475.

Brunger, A. T., Adams, P. D., Clore, G. M., DeLano, W. L., Gros, P., Grosse-Kunstleve, W., Jian, J., Kuszewski, J., Nilges, M., Pannu, N. S., Read, R. J., Rice, L. M., Simonson, T. & Warren, G. L. (1998). Crystallography and NMR system (CNS): a new software suite for macromolecular structure determination. *Acta. Crystallog. sect. D*, 54, 905-921.

Cambillau, C. & Horjales, E. (1987). TOM: a FRODO subpackage for protein-ligand fitting with interactive energy minimization. *J. Mol. Graph.* 5, 175-177.

Carson, M. (1991). Ribbons 2. 0. *J. Appl. Crystallog.* 24, 958-961.

CCP4. (1994). The CCP4 Suite: programs for protein crystallography. *Acta Crystallog. sect. D*, 50, 760-763.

Chang, N. T., Kung, H-F. & Pestka, S. (1983). Synthesis of a human leukocyte interferon with a modified carboxy terminus in *Escherichia coli*. *Arch. Biochem. Biophys.* 221(2), 585-589.

Cheetham, B. F., McInnes, B., Mantamadiotis, T., Murray, P. J., Ålin Per Bourke, P., Linnane, A. W. & Tymms, M. J. (1991). Structure-function studies of human interferon-α: enhanced activity on human and murine cells. *Antiviral Res.* 15, 27-40.

Cohen, B., Novick, D., Barak, S. & Rubinstein, M. (1995). Ligand-induced association of the type I interferon receptor components. *Mol. Cell. Biol.* 15, 4208-4214.

Colamonici, O. R., Platanias, L. C., Domanski, P., Handa, R., Gilmour, K. C., Diaz, M. O., Reich, N. & Pitha-Rowe, P. (1996). Transmembrane signaling by the α subunit of the type I interferon receptor is essential for activation of the jak kinases and the transcriptional factor ISGF3. *J. Biol. Chem.* 270(14), 8188-8193.

Cook, J. R., Cleary, C. M., Mariano, T. M., Izotova, L. & Pestka, S. (1996). Differential responsiveness of a splice variant of the human type I interferon receptor to interferons. *J. Biol. Chem.* 271(23), 13448-13453.

Cowtan, K. (1994). 'DM' an automated procedure for phase improvement by density modification. In *Joint CCP4 and ESF: EACBM Newsletter on Protein Crystallography* (Bailey, S. & Wilson, K., eds), vol. 31, pp. 34-38, Dansbury Laboratory, Hamburg, Germany.

de Vos, A. M., Ultsch, M. & Kossiakoff, A. A. (1991). Human growth hormone and extracellular domain of its receptor: crystal structure of the complex. *Science*, 255, 306-312.

Domanski, P., Witte, M., Kellum, M., Rubinstein, M., Hackett, R., Pitha, P. & Colmonici, (1995). Cloning and expression of a long form of the β subunit of the interferon αβ receptor that is required for signaling. *J. Biol. Chem.* 270(37), 21606-21611.

Engh, R. A. & Huber, R. (1991). Accurate bond and angle parameters for X-ray protein structure refinement. *Acta Crystallog. sect. A*, 47, 392-400.

Godkin, J. D., Bazer, F. W., Moffatt, J., Sessions, F. & Roberts, R. M. (1982). Purification and properties of a major, low molecular weight protein released by the trophoblast of sheep blastocysts at Day 13-21. *J. Reprod. Fert.* 65, 141-150.

Imakawa, K., Anthony, R. V., Kazemin, M., Marotti, K. R., Polites, H. G. & Roberts, R. M. (1987). Interferon-like sequence of ovine trophoblast protein secreted by embryonic trophectoderm. *Nature*, 330, 377-379.

Jarpe, M. A., Johnson, H. M., Bazer, F. W., Ott, T. L., Curto, E. V., Krishna, N. R. & Pontzer, C. H. (1994). Predicted structural motif of IFNτ. *Protein Eng.* **7**(7), 863-867.

Jiang, J.-S. & Brunger, A. T. (1994). Protein hydration observed by X-ray diffraction. Solvation properties of penicillopepsin and neuraminidase crystal structures. *J. Mol. Biol.* **243**, 100-115.

Jones, A. T. & Kjeldgaard, M. (1993). *O-The Manual, Version 5.9*, Uppsala, Sweden.

Kabsch, W. (1976). A solution of the best rotation to relate two sets of vectors. *Acta Crystallog. sect. A*, **32**, 922-923.

Karpusas, M., Nolte, M., Benton, C. B., Meier, W., Lipscomb, W. N. & Goelz, S. (1997). The crystal structure of human interferon β at 2.2-Å resolution. *Proc. Natl Acad. Sci. USA*, **94**, 11813-11818.

Laskowski, R. J., Macarthur, M. W., Moss, D. S. & Thronton, J. M. (1993). Procheck: a program to check stereochemical quality of protein structures. *J. Appl. Crystallog.* **26**, 283-290.

Li, J. & Roberts, R. M. (1994a). Structure-function relationships in the interferon-τ (IFN-τ). *J. Biol. Chem*, **269**, (**18**), 13544-13550.

Li, J. & Roberts, R. M. (1994b). Interferon-τ and interferon-α interact with the same receptors in bovine endometroium. *J. Biol. Chem.* **269**(**40**), 24826-24833.

Matthews, B. W. (1968). Solvent content of protein crystals. *J. Mol. Biol.* **33**, 491-497.

Mitsui, Y., Senda, T., Shimazu, T., Matsuda, S. & Utsumi, J. (1993). Structural, functional and evolutionary implications of the three-dimensional crystal structure of murine interferon-β. *Pharmacol. Ther.* **58**, 93-132.

Nagabhushan, T. L. & Giaquinto, A. (1995). *Biopharmaceutical Production* (Lubiniecki, A. S. & Vargo, S. A., eds), pp. 221-234, John Wiley & Sons, New York, NY.

Navaza, J. (1994). AMoRe: an automated package for molecular replacement. *Acta Crystallog. sect. A*, **50**, 157-163.

Ott, T. L., Van Heeke, G., Johnson, H. M. & Bazer, F. W. (1991). Cloning and expression in *Saccharomyces cerevisiae* of a synthetic gene for the type-I trophoblast interferon ovine trophoblast protein-1: purification and antiviral activity. *J. Interferon Res.* **11**, 357-364.

Otwinowski, Z. (1991). Maximum likehood refinement of heavy-atom parameters. In *Isomorphous Replacement and Anomalous Scatterings: Proceedings of the CCP4 Study Weekend* (Wolf, W., Evan, P. R. & Leslie, A. G. W., eds), pp. 23-38.

Otwinowski, Z. (1993). Oscillation data reduction program. In *Data Collection and Processing: Proceedings of the CCP4 Study Weekend* (Sawyer, L., Isaacs, N. & Bailey, S., eds).

Pannu, N. S. & Read, R. J. (1996). Improved structure refinement through maximum likelihood. *Acta Crystallog. sect. A*, **52**, 659-668.

Pellegrini, S. & Dusanter-Fourt, I. (1997). The structure, regulation and function of the Janus kinases (JAKs) and the signal transducers and activators of transcription (STATs). *Eur. J. Biochem.* **248**(3), 615-633.

Pestka, S. (1997). The human interferon-α species and hybrid proteins. *Semin. Oncol.* **24**(**S9**), 4-17.

Petricoin, E. F., Ito, S., Williams, B. L., Audet, S., Stancato, L. F., Gamero, A., Clouse, K., Grimley, P., Weiss, A., Beeler, J., Finbloom, D. S., Shores, E. W., Abraham, R. & Larner, A. C. (1997). Antiproliferative action of interferon-a requires component of T-cell-receptor signalling. *Nature*, 390, 629-632.

Pontzer, C. H., Torres, B. A., Vallet, J. L., Bazer, F. W. & Johnson, H. M. (1988). Antiviral activity of the pregnancy recognition hormone ovine trophoblast protein-1. *Biochem. Biophys. Res. Commun.* 152(2), 801-807.

Pontzer, C. H., Ott, T. L., Bazer, F. W. & Johnson, H. M. (1990). Localization of an antiviral site on the pregnancy recognition hormone, ovine trophoblast protein 1. *Proc. Natl Acad. Sci. USA*, 87, 5945-5949.

Pontzer, C. H., Bazer, F. W. & Johnson, H. M. (1991). Antiproliferative activity of a pregnancy recognition hormone, ovine trophoblast protein-1. *Cancer Res.* **51**, 5304-5307.

Pontzer, C. H., Ott, T. L., Bazer, F. W. & Johnson, H. M. (1994). Structure/function studies with interferon tau: evidence for multiple active sites. *J. Interferon Res.* **14**, 133-141.

Presnell, S. R. & Cohen, F. R. (1989). Topological distribution of four-alpha-helix bundles. *Proc. Natl Acad. Sci. USA*, **86**, 6592-6596.

Radhakrishnan, R., Walter, L. J., Hruza, A., Reichert, P., Trotta, P. P., Nagabhushan, T. L. & Walter, M. R. (1996). Zinc mediated dimer of human interferon-α_{2b} revealed by X-ray crystallography. *Structure*, **4**, 1453-1463.

Read, R. J. (1986). Improved fourier coefficients for maps using phases from partial structures with errors. *Acta Crystallog. sect. A*, **42**, 140-149.

Rehberg, E., Kelder, B., Hoal, E. G. & Pestka, S. (1982). Specific molecular activities of recombinant and hybrid leukocyte interferons. *J. Biol. Chem.* **257**, 11497-11502.

Rice, L. M. & Brunger, A. T. (1994). Torsion angle dynamics: reduced variable conformational sampling enhances crystallogrphic structure refinement. *Proteins: Struct. Funct. Genet.* **19**, 277-290.

Roberts, R. M. (1991). A role for interferons in early pregnancy. *BioEssays*, **13**(**3**), 121-126.

Roberts, R. M., Cross, J. C. & Leaman, D. W. (1991). Unique features of the trophoblast interferons. *Pharmacol. Ther.* **51**, 329-345.

Roberts, R. M., Cross, J. C. & Leaman, D. W. (1992). Interferons as hormones of pregnancy. *Endocrine Rev.* **13**, 432-452.

Sack, J. S. (1988). CHAIN: a crystallographic modeling package. *J. Mol. Graph.* **6**, 224-225.

Senda, T., Saitoh, S.-I. & Mitsui, Y. (1995a). Refined crystal structure of recombinant murine interferon-β at 2.15 Å resolution. *J. Mol. Biol.* **253**, 187-207.

Senda, T., Saitoh, S.-I., Mitsui, Y., Li, J. & Roberts, R. M. (1995b). A three-dimensional model of interferon-τ. *J. Interferon Res.* **15**, 1053-106.

Seto, M. H., Harkins, R. N., Adler, M., Whitlow, M., Church, W. B. & Croze, E. (1995). Homology model of human interferon-α8 and its receptor complex. *Protein Sci.* **4**, 655-670.

Sprang, S. & Bazan, J. F. (1993). Cytokines structural taxonomy and mechanisms of receptor engagement. *Curr. Opin. Struct. Biol.* 3, 815-827.

Strander, H. A. (1989). Clinical effects of interferon therapy with special emphasis on antitumor efficacy. *Acta Oncol.* **28**, 355-362.

Subramaniam, P. S., Khan, S. A., Pontzer, C. H. & Johnson, H. M. (1995). Differential recognition of the type I interferon receptor by interferons τ and α is responsible for their disparate cytotoxicities. *Proc. Natl Acad. Sci. USA*, **92**, 12270-12274.

Uzé, G., Luttalla, G. & Gresser, I. (1990). Genetic transfer of a functional human interferon α receptor into mouse cells: cloning and expression of its cDNA. *Cell*, 60, 225-234.

Uzé, G., Di Marco, S., Mouchel-Vielh, E., Monneron, D., Bandu, M.-T., Horisberger, M. A., Dorques, A., Lutfalla, G. & Mogenson, K. E. (1994). Domains of interaction between alpha interferon and its receptor components. *J. Mol. Biol.* 243, 245-257.

Walter, M. R. & Nagabhushan, T. L. (1995). Crystal structure of interleukin 10 reveals an interferon γ-like fold. *Biochemistry*, 34, 12118-12125.

Walter, M. R., Windsor, W. T., Nagabhushan, T. L., Lundell, D. J., Lunn, C. A., Zauodny, P. J. & Narula, S. K. (1995). Crystal structure of a complex between interferon-γ and its soluble high-affinity receptor. *Nature*, 376, 230-235.

Weber, H., Valenzuela, D., Lujber, G., Gubler, M. & Weissman, C. (1987). Single amino acid changes that render human IFN-α_2 biologically active on mouse cells. *EMBO J.* 6, 591-598.

Wisconsin Package Version 9.0, Genetics Computer Group (GCG), Madison, Wisc.

Edited by R. Huber

(Received 10 June 1998; received in revised form 20 November 1998; accepted 3 December 1998)